Chapter 7

# Geostrophic Flows and Vorticity Dynamics

**ABSTRACT**
This chapter treats homogeneous flows with small Rossby and Ekman numbers. It is shown that such flows have a tendency to display vertical rigidity. The concept of potential vorticity is then introduced. The solution of vertically homogeneous flows often involves a Poisson equation for the pressure distribution, and numerical techniques are presented for this purpose.

## 7.1 HOMOGENEOUS GEOSTROPHIC FLOWS

Let us consider rapidly rotating fluids by restricting our attention to situations where the Coriolis acceleration strongly dominates the various acceleration terms. Let us further consider homogeneous fluids and ignore frictional effects, by assuming

$$Ro_T \ll 1, \quad Ro \ll 1, \quad Ek \ll 1, \tag{7.1}$$

together with $\rho = 0$ (no density variation). The lowest-order equations governing such homogeneous, frictionless, rapidly rotating fluids are the following simplified forms of equations of motion, Eq. (4.21):

$$-fv = -\frac{1}{\rho_0}\frac{\partial p}{\partial x} \tag{7.2a}$$

$$+fu = -\frac{1}{\rho_0}\frac{\partial p}{\partial y} \tag{7.2b}$$

$$0 = -\frac{1}{\rho_0}\frac{\partial p}{\partial z} \tag{7.2c}$$

$$\frac{\partial u}{\partial x} + \frac{\partial v}{\partial y} + \frac{\partial w}{\partial z} = 0, \tag{7.2d}$$

where $f$ is the Coriolis parameter.

This reduced set of equations has a number of surprising properties. First, if we take the vertical derivative of the first equation, (7.2a), we obtain,

**Introduction to Geophysical Fluid Dynamics,** Volume 101, ISSN 0074-6142, DOI: 10.1016/B978-0-12-088759-0.00007-9

successively,

$$-f\frac{\partial v}{\partial z}=-\frac{1}{\rho_0}\frac{\partial}{\partial z}\left(\frac{\partial p}{\partial x}\right)=-\frac{1}{\rho_0}\frac{\partial}{\partial x}\left(\frac{\partial p}{\partial z}\right)=0,$$

where the right-hand side vanishes because of Eq. (7.2c). The other horizontal momentum equation, (7.2b), succumbs to the same fate, bringing us to conclude that the vertical derivative of the horizontal velocity must be identically zero:

$$\frac{\partial u}{\partial z}=\frac{\partial v}{\partial z}=0. \tag{7.3}$$

This result is known as the *Taylor–Proudman theorem* (Proudman, 1953; Taylor, 1923). Physically, it means that the horizontal velocity field has no vertical shear and that all particles on the same vertical move in concert. Such vertical rigidity is a fundamental property of rotating homogeneous fluids.

Next, let us solve the momentum equations in terms of the velocity components, a trivial task:

$$u=\frac{-1}{\rho_0 f}\frac{\partial p}{\partial y},\qquad v=\frac{+1}{\rho_0 f}\frac{\partial p}{\partial x}, \tag{7.4}$$

with the corollary that the vector velocity $(u, v)$ is perpendicular to the vector $(\partial p/\partial x, \partial p/\partial y)$. Since the latter vector is none other than the pressure gradient, we conclude that the flow is not down-gradient but rather across-gradient. The fluid particles are not cascading from high to low pressures, as they would in a nonrotating viscous flow but, instead, are navigating along lines of constant pressure, called *isobars* (Fig. 7.1). The flow is said to be isobaric, and isobars are streamlines. It also implies that no pressure work is performed either on the fluid or by the fluid. Hence, once initiated, the flow can persist without a continuous source of energy.

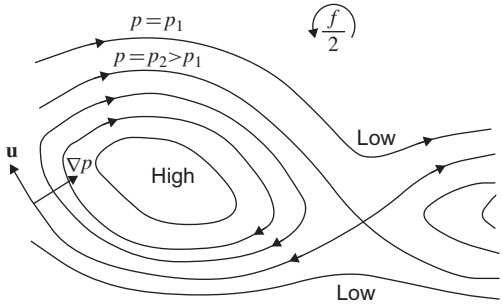


**FIGURE 7.1** Example of geostrophic flow. The velocity vector is everywhere parallel to the lines of equal pressure. Thus, pressure contours act as streamlines. In the northern hemisphere (as pictured here), the fluid circulates with the high pressure on its right. The opposite holds for the southern hemisphere.

Such a flow field, where a balance is struck between the Coriolis and pressure forces, is called *geostrophic* (from the Greek, $\gamma\eta$ = Earth and $\sigma\tau\rho o\varphi\eta$ = turning). The property is called *geostrophy*. Hence, by definition, all geostrophic flows are isobaric.

A remaining question concerns the direction of flow along pressure lines. A quick examination of the signs in expressions (7.4) reveals that where $f$ is positive (northern hemisphere, counterclockwise ambient rotation), the currents/winds flow with the high pressures on their right. Where $f$ is negative (southern hemisphere, clockwise ambient rotation), they flow with the high pressures on their left. Physically, the pressure force is directed from the high pressure toward the low pressure initiating a flow in that direction, but on the rotating planet, this flow is deflected to the right (left) in the northern (southern) hemisphere. Figure 7.2 provides a meteorological example from the northern hemisphere.

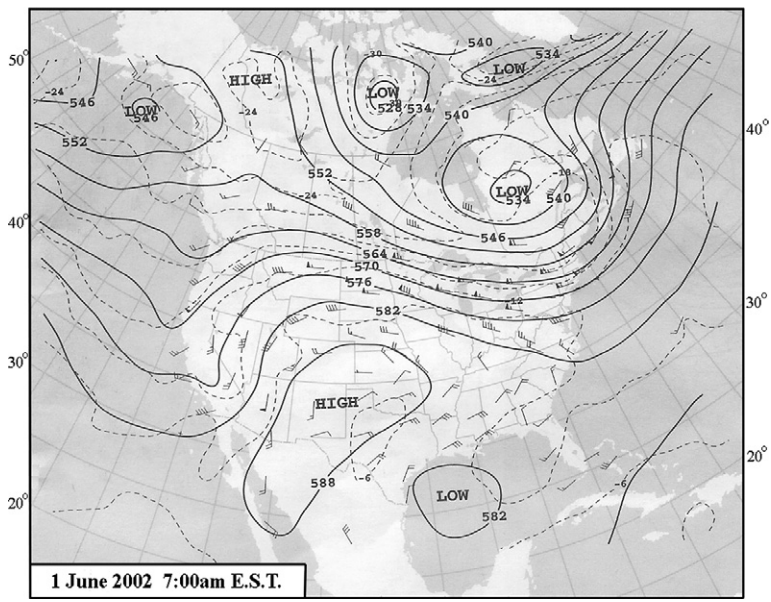


**FIGURE 7.2** A meteorological example showing the high degree of parallelism between wind velocities and pressure contours (isobars), indicative of geostrophic balance. The solid lines are actually height contours of a given pressure (500 mb in this case) and not pressure at a given height. However, because atmospheric pressure variations are large in the vertical and weak in the horizontal, the two sets of contours are nearly identical by virtue of the hydrostatic balance. According to meteorological convention, wind vectors are depicted by arrows with flags and barbs: on each tail, a flag indicates a speed of 50 knots, a barb 10 knots, and a half-barb 5 knots (1 knot = 1 nautical mile per hour = 0.5144 m/s). The wind is directed toward the bare end of the arrow because meteorologists emphasize where the wind comes from, not where it is blowing. The dashed lines are isotherms. (*Chart by the National Weather Service, Department of Commerce, Washington, D.C.*)

If the flow field extends over a meridional span that is not too wide, the variation of the Coriolis parameter with latitude is negligible, and $f$ can be taken as a constant. The frame of reference is then called the *f-plane*. In this case, the horizontal divergence of the geostrophic flow vanishes:

$$\frac{\partial u}{\partial x}+\frac{\partial v}{\partial y}=-\frac{\partial}{\partial x}\left(\frac{1}{\rho_0 f}\frac{\partial p}{\partial y}\right)+\frac{\partial}{\partial y}\left(\frac{1}{\rho_0 f}\frac{\partial p}{\partial x}\right)=0. \tag{7.5}$$

Hence, geostrophic flows are naturally nondivergent on the $f$-plane. This leaves no room for vertical convergence or divergence, as the continuity equation (7.2d) implies:

$$\frac{\partial w}{\partial z}=0. \tag{7.6}$$

A corollary is that the vertical velocity, too, is independent of height. If the fluid is limited in the vertical by a flat bottom (horizontal ground or sea for the atmosphere) or by a flat lid (sea surface for the ocean), this vertical velocity must simply vanish, and the flow is strictly two-dimensional.

## 7.2 HOMOGENEOUS GEOSTROPHIC FLOWS OVER AN IRREGULAR BOTTOM

Let us still consider a rapidly rotating fluid so that the flow is geostrophic, but now over an irregular bottom. We neglect the possible surface displacements, assuming that they remain modest in comparison with the bottom irregularities (Fig. 7.3). An example would be the flow in a shallow sea (homogeneous waters) with depth ranging from 20 to 50 m and under surface waves a few centimeters high.

As shown in the development of kinematic boundary conditions (4.28), if the flow were to climb up or down the bottom, it would undergo a vertical velocity proportional to the slope:

$$w=u\frac{\partial b}{\partial x}+v\frac{\partial b}{\partial y}, \tag{7.7}$$

where $b$ is the bottom elevation above the reference level. The analysis of the previous section implies that the vertical velocity is constant across the entire

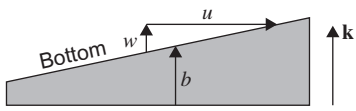


**FIGURE 7.3** Schematic view of a flow over a sloping bottom. A vertical velocity must accompany flow across isobaths.

depth of the fluid. Since it must be zero at the top, it must be so at the bottom as well; that is,

$$u\frac{\partial b}{\partial x}+v\frac{\partial b}{\partial y}=0, \tag{7.8}$$

and the flow is prevented from climbing up or down the bottom slope. This property has profound implications. In particular, if the topography consists of an isolated bump (or dip) in an otherwise flat bottom, the fluid on the flat bottom cannot rise onto the bump, even partially, but must instead go around it. Because of the vertical rigidity of the flow, the fluid parcels at all levels—including levels above the bump elevation—must likewise go around. Similarly, the fluid over the bump cannot leave the bump but must remain there. Such permanent tubes of fluids trapped above bumps or cavities are called *Taylor columns* (Taylor, 1923).

In flat-bottomed regions, a geostrophic flow can assume arbitrary patterns, and the actual pattern reflects the initial conditions. But over a bottom where the slope is nonzero almost everywhere (Fig. 7.4), the geostrophic flow has no choice but to follow the depth contours (called *isobaths*). Pressure contours are then aligned with topographic contours, and isobars coincide with isobaths. These lines are sometimes also called *geostrophic contours*. Note that a relation between pressure and fluid thickness exists but cannot be determined without additional information on the flow.

Open isobaths that start and end on a side boundary cannot support any flow, otherwise fluid would be required to enter or leave through lateral boundaries. The flow is simply blocked along the entire length of these lines. In other words, geostrophic flow can occur only along closed isobaths.

The preceding conclusions hold true as long as the upper boundary is horizontal. If this is not the case, it can then be shown that geostrophic flows are

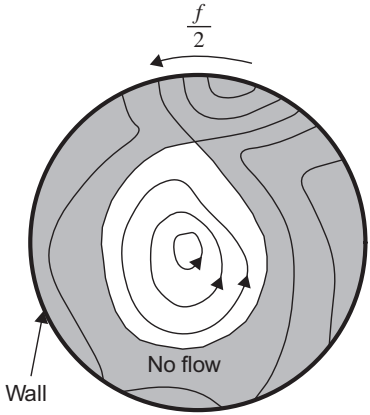


**FIGURE 7.4** Geostrophic flow in a closed domain and over irregular topography. Solid lines are isobaths (contours of equal depth). Flow is permitted only along closed isobaths.

constrained to be directed along lines of constant fluid depth. (See Analytical Problem 7.3.) Thus, the fluid is allowed to move up and down, but only as long as it is not being vertically squeezed or stretched. This property is a direct consequence of the inability of geostrophic flows to undergo any two-dimensional divergence.

## 7.3 GENERALIZATION TO NONGEOSTROPHIC FLOWS

Let us now suppose that the fluid is not rotating as rapidly so that the Coriolis acceleration no longer dwarfs other acceleration terms. We still continue to suppose that the fluid is homogeneous and frictionless. The momentum equations are now augmented to include the relative acceleration terms:

$$\frac{\partial u}{\partial t}+u\frac{\partial u}{\partial x}+v\frac{\partial u}{\partial y}+w\frac{\partial u}{\partial z}-fv=-\frac{1}{\rho_0}\frac{\partial p}{\partial x} \tag{7.9a}$$

$$\frac{\partial v}{\partial t}+u\frac{\partial v}{\partial x}+v\frac{\partial v}{\partial y}+w\frac{\partial v}{\partial z}+fu=-\frac{1}{\rho_0}\frac{\partial p}{\partial y}. \tag{7.9b}$$

Pressure still obeys (7.2c), and continuity equation (7.2d) has not changed.

If the horizontal flow field is initially independent of depth, it will remain so at all future times. Indeed, the nonlinear advection terms and the Coriolis terms are initially $z$-independent, and the pressure terms are, too, $z$-independent by virtue of Eq. (7.2c). Thus, $\partial u/\partial t$ and $\partial v/\partial t$ must be $z$-independent, which implies that $u$ and $v$ tend not to become depth varying and thus remain $z$-independent at all subsequent times. Let us restrict our attention to such flows, which in the jargon of geophysical fluid dynamics are called *barotropic*. Equations (7.9) then reduce to

$$\frac{\partial u}{\partial t}+u\frac{\partial u}{\partial x}+v\frac{\partial u}{\partial y}-fv=-\frac{1}{\rho_0}\frac{\partial p}{\partial x} \tag{7.10a}$$

$$\frac{\partial v}{\partial t}+u\frac{\partial v}{\partial x}+v\frac{\partial v}{\partial y}+fu=-\frac{1}{\rho_0}\frac{\partial p}{\partial y}. \tag{7.10b}$$

Although the flow has no vertical structure, the similarity to geostrophic flow ends here. In particular, the flow is not required to be aligned with the isobars or it is devoid of vertical velocity. To determine the vertical velocity, we turn to continuity equation (7.2d),

$$\frac{\partial u}{\partial x}+\frac{\partial v}{\partial y}+\frac{\partial w}{\partial z}=0,$$

in which we note that the first two terms are independent of $z$ but do not necessarily add up to zero. A vertical velocity varying linearly with depth can exist, enabling the flow to support two-dimensional divergence and thus allowing a flow across isobaths.

An integration of the preceding equation over the entire fluid depth yields

$$\left(\frac{\partial u}{\partial x}+\frac{\partial v}{\partial y}\right)\int_b^{b+h} \mathrm{d}z + [w]_b^{b+h} = 0, \tag{7.11}$$

where $b$ is the bottom elevation above a reference level, and $h$ is the local and instantaneous fluid layer thickness (Fig. 7.5). Because fluid particles on the surface cannot leave the surface and particles on the bottom cannot penetrate through the bottom, the vertical velocities at these levels are given by Eqs. (4.28) and (4.31)

$$\begin{aligned} w(z=b+h) &= \frac{\partial}{\partial t}(b+h)+u\frac{\partial}{\partial x}(b+h)+v\frac{\partial}{\partial y}(b+h) \\ &= \frac{\partial \eta}{\partial t}+u\frac{\partial \eta}{\partial x}+v\frac{\partial \eta}{\partial y} \end{aligned} \tag{7.12}$$

$$w(z=b) = u\frac{\partial b}{\partial x}+v\frac{\partial b}{\partial y}. \tag{7.13}$$

Equation (7.11) then becomes, using the surface elevation $\eta = b+h-H$:

$$\frac{\partial \eta}{\partial t}+\frac{\partial}{\partial x}(hu)+\frac{\partial}{\partial y}(hv)=0, \tag{7.14}$$

which supersedes Eq. (7.2d) and eliminates the vertical velocity from the formalism.

Finally, since the fluid is homogeneous, the dynamic pressure, $p$, is independent of depth. In the absence of a pressure variation above the fluid surface (e.g., uniform atmospheric pressure over the ocean), this dynamic pressure is

$$p = \rho_0 g \eta, \tag{7.15}$$

where $g$ is the gravitational acceleration according to (4.33). With $p$ replaced by the preceding expression, Eqs. (7.10) and (7.14) form a 3-by-3 system for the variables $u$, $v$, and $\eta$. The vertical variable no longer appears, and the

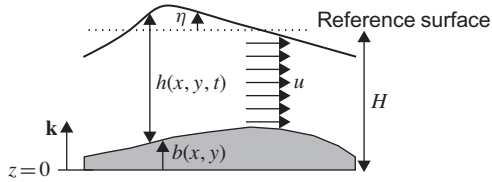


**FIGURE 7.5** Schematic diagram of unsteady flow of a homogeneous fluid over an irregular bottom and the attending notation.

independent variables are $x$, $y$, and $t$. This system is

$$\frac{\partial u}{\partial t}+u\frac{\partial u}{\partial x}+v\frac{\partial u}{\partial y}-fv=-g\frac{\partial \eta}{\partial x} \tag{7.16a}$$

$$\frac{\partial v}{\partial t}+u\frac{\partial v}{\partial x}+v\frac{\partial v}{\partial y}+fu=-g\frac{\partial \eta}{\partial y} \tag{7.16b}$$

$$\frac{\partial \eta}{\partial t}+\frac{\partial}{\partial x}(hu)+\frac{\partial}{\partial y}(hv)=0. \tag{7.16c}$$

Although this system of equations is applied as frequently to the atmosphere as to the ocean, it bears the name *shallow-water model*.[1] If the bottom is flat, the equations become

$$\frac{\partial u}{\partial t}+u\frac{\partial u}{\partial x}+v\frac{\partial u}{\partial y}-fv=-g\frac{\partial h}{\partial x} \tag{7.17a}$$

$$\frac{\partial v}{\partial t}+u\frac{\partial v}{\partial x}+v\frac{\partial v}{\partial y}+fu=-g\frac{\partial h}{\partial y} \tag{7.17b}$$

$$\frac{\partial h}{\partial t}+\frac{\partial}{\partial x}(hu)+\frac{\partial}{\partial y}(hv)=0. \tag{7.17c}$$

This is a formulation that we will encounter in layered models (Chapter 12).

## 7.4 VORTICITY DYNAMICS

In the study of geostrophic flows (Section 7.1), it was noted that the pressure terms cancel in the expression of the two-dimensional divergence. Let us now repeat this operation while keeping the added acceleration terms by subtracting the $y$-derivative of Eq. (7.10a) from the $x$-derivative of Eq. (7.10b). After some manipulations, the result can be cast as follows:

$$\frac{\mathrm{d}}{\mathrm{d}t}\left(f+\frac{\partial v}{\partial x}-\frac{\partial u}{\partial y}\right)+\left(\frac{\partial u}{\partial x}+\frac{\partial v}{\partial y}\right)\left(f+\frac{\partial v}{\partial x}-\frac{\partial u}{\partial y}\right)=0, \tag{7.18}$$

where the material time derivative is defined as

$$\frac{\mathrm{d}}{\mathrm{d}t}=\frac{\partial}{\partial t}+u\frac{\partial}{\partial x}+v\frac{\partial}{\partial y}.$$

[1] In the absence of rotation, these equations also bear the name of *Saint-Venant equations*, in honor of Jean Claude Barré de Saint-Venant (1797–1886) who first derived them in the context of river hydraulics.

In the derivation, care was taken to allow for the possibility of a variable Coriolis parameter (which on a sphere varies with latitude and thus with position). The grouping

$$f+\frac{\partial v}{\partial x}-\frac{\partial u}{\partial y}=f+\zeta \tag{7.19}$$

is interpreted as the sum of the ambient vorticity ($f$) with the relative vorticity ($\zeta=\partial v/\partial x-\partial u/\partial y$). To be precise, the vorticity is a vector, but since the horizontal flow field has no depth dependence, there is no vertical shear and no eddies with horizontal axes. The vorticity vector is strictly vertical, and the preceding expression merely shows that vertical component.

Similarly, terms in the continuity equation, (7.14), can be regrouped as

$$\frac{\mathrm{d}}{\mathrm{d}t}h+\left(\frac{\partial u}{\partial x}+\frac{\partial v}{\partial y}\right)h=0. \tag{7.20}$$

If we now consider a narrow fluid column of horizontal cross-section d$s$, its volume is $h$d$s$, and by virtue of conservation of volume in an incompressible fluid, the following equation holds:

$$\frac{\mathrm{d}}{\mathrm{d}t}(h\,\mathrm{d}s)=0. \tag{7.21}$$

This implies, as intuition suggests, that if the parcel is squeezed vertically (decreasing $h$), it stretches horizontally (increasing d$s$), and vice versa (Fig. 7.6). Combining Eq. (7.20) for $h$ with Eq. (7.21) for $h$d$s$ yields an equation for d$s$:

$$\frac{\mathrm{d}}{\mathrm{d}t}\mathrm{d}s=\left(\frac{\partial u}{\partial x}+\frac{\partial v}{\partial y}\right)\mathrm{d}s, \tag{7.22}$$

which simply says that horizontal divergence ($\partial u/\partial x+\partial v/\partial y>0$) causes widening of the cross-sectional area d$s$, and convergence ($\partial u/\partial x+\partial v/\partial y<0$) a

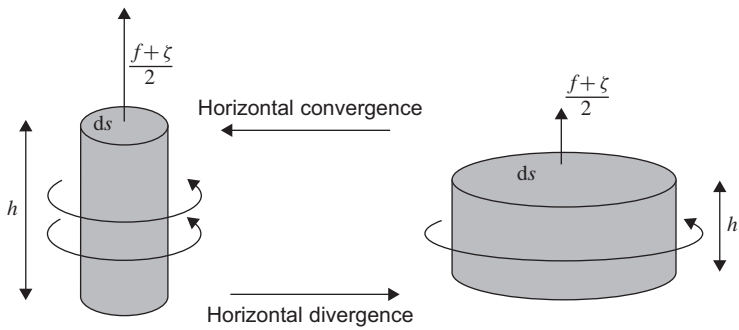


**FIGURE 7.6** Conservation of volume and circulation of a fluid parcel undergoing vertical squeezing or stretching. The products $h$d$s$ and $(f+\zeta)$d$s$ are conserved during the transformation. As a corollary, the ratio $(f+\zeta)/h$, called the potential vorticity, is also conserved.

narrowing of the cross-section. It could have been derived from first principles (see Analytical Problem 7.4).

Now, combining Eqs. (7.18) and (7.22) yields

$$\frac{\mathrm{d}}{\mathrm{d}t}[(f+\zeta)\mathrm{d}s]=0 \tag{7.23}$$

and implies that the product $(f+\zeta)\mathrm{d}s$ is conserved by the fluid parcel. This product can be interpreted as the vorticity flux (vorticity integrated over the cross section) and is therefore the *circulation* of the parcel. Equation (7.23) is the particular expression for rotating, two-dimensional flows of Kelvin's theorem, which guarantees conservation of circulation in inviscid fluids (Kundu, 1990, pages 124–128).

This conservation principle is akin to that of angular momentum for an isolated system. The best example is that of a ballerina spinning on her toes; with her arms stretched out, she spins slowly, but with her arms brought against her body, she spins more rapidly. Likewise in homogeneous geophysical flows, when a parcel of fluid is squeezed laterally ($\mathrm{d}s$ decreasing), its vorticity must increase ($f+\zeta$ increasing) to conserve circulation.

Now, if both circulation and volume are conserved, so is their ratio. This ratio is particularly helpful, for it eliminates the parcel's cross section and thus depends only on local variables of the flow field:

$$\frac{\mathrm{d}}{\mathrm{d}t}\left(\frac{f+\zeta}{h}\right)=0, \tag{7.24}$$

where

$$q=\frac{f+\zeta}{h}=\frac{f+\partial v/\partial x-\partial u/\partial y}{h} \tag{7.25}$$

is called the *potential vorticity*. The preceding analysis interprets potential vorticity as circulation per volume. This quantity, as will be shown on numerous occasions in this book, plays a fundamental role in geophysical flows. Note that equation (7.24) could have been derived directly from Eqs. (7.18) and (7.20) without recourse to the introduction of the variable $\mathrm{d}s$.

Let us now go full circle and return to rapidly rotating flows, those in which the Coriolis force dominates. In this case, the Rossby number is much less than unity ($Ro=U/\Omega L\ll 1$), which implies that the relative vorticity ($\zeta=\partial v/\partial x-\partial u/\partial y$, scaling as $U/L$) is negligible in front of the ambient vorticity ($f$, scaling as $\Omega$). The potential vorticity reduces to

$$q=\frac{f}{h}, \tag{7.26}$$

which, if $f$ is constant—such as in a rotating laboratory tank or for geophysical patterns of modest meridional extent—implies that each fluid column must

conserve its height $h$. In particular, if the upper boundary is horizontal, fluid parcels must follow isobaths, consistent with the existence of Taylor columns (Section 7.2). If $f$ is variable (see also Section 9.4) and topography flat, the same constraint (7.26) tells us that the flow cannot cross latitudinal circles, while in the general case, the flow must follow lines of constant $f/h$.

Before closing this section, let us derive a germane result, which will be useful later. Consider the dimensionless expression

$$\sigma = \frac{z-b}{h}, \tag{7.27}$$

which is the fraction of the local height above the bottom to the full depth of the fluid, or, in short, the relative height above bottom ($0 \leq \sigma \leq 1$). This expression will later be defined as the so-called $\sigma$-coordinate (see Section 20.6.1). Its material time derivative is

$$\frac{\mathrm{d}\sigma}{\mathrm{d}t} = \frac{1}{h}\frac{\mathrm{d}}{\mathrm{d}t}(z-b) - \frac{z-b}{h^2}\frac{\mathrm{d}h}{\mathrm{d}t}. \tag{7.28}$$

Since $\mathrm{d}z/\mathrm{d}t = w$ by definition of the vertical velocity and because $w$ varies linearly from $\mathrm{d}b/\mathrm{d}t$ at the bottom ($z=b$) to $d(b+h)/\mathrm{d}t$ at the top ($z=b+h$), we have

$$\frac{\mathrm{d}z}{\mathrm{d}t} = w = \frac{\mathrm{d}b}{\mathrm{d}t} + \frac{z-b}{h}\frac{\mathrm{d}h}{\mathrm{d}t}. \tag{7.29}$$

Use of this last expression to eliminate $\mathrm{d}z/\mathrm{d}t$ from Eq. (7.28) cancels all terms on the right, leaving only

$$\frac{\mathrm{d}\sigma}{\mathrm{d}t} = 0. \tag{7.30}$$

Thus, a fluid parcel retains its relative position within the fluid column. Even if there is a vertical velocity, the structure of the velocity field is such that layers of fluid remain invariably stacked on each other. Hence, there is no internal overturning, and layers are simply squeezed or stretched.

## 7.5 RIGID-LID APPROXIMATION

Except in the case when fast surface waves are of interest (Section 9.1), we can exploit the fact that large-scale motions in the ocean are relatively slow and introduce the so-called rigid-lid approximation. Large-scale movements with small Rossby numbers are close to geostrophic equilibrium, and their dynamic pressure thus scales as $p \sim \rho_0 \Omega U L$ (see (4.16)), and since $p = \rho_0 g \eta$ in a homogeneous fluid, the scale $\Delta H$ of surface-height displacements is $\Delta H \sim \Omega U L/g$. Using the latter in the vertically integrated volume-conservation equation, we can then compare the sizes of the different terms. Assuming that the timescale

is not shorter than the inertial timescale $1/\Omega$, we have

$$\frac{\partial \eta}{\partial t} + \frac{\partial}{\partial x}(hu) + \frac{\partial}{\partial y}(hv) = 0$$
$$\Omega \Delta H \qquad \frac{HU}{L} \qquad \frac{HU}{L},$$

in which $\Omega \Delta H \sim \Omega^2 UL/g$, and the scale ratio of the first term to the other terms is $\Omega^2 L^2/gH$. In many situations, this ratio is very small,

$$\frac{\Omega^2 L^2}{gH} \ll 1, \tag{7.31}$$

and the time derivative in the volume-conservation equation may be neglected:

$$\frac{\partial}{\partial x}(hu) + \frac{\partial}{\partial y}(hv) = 0. \tag{7.32}$$

This is called the *rigid-lid approximation* (Fig. 7.7).

However, this approximation has a major implication when we solve the equations numerically because now, instead of using the time derivative of the continuity equation to march $\eta$ forward in time and determine the hydrostatic pressure $p$ from it, we somehow need to find a pressure field that ensures that at any moment the *transport* field $(\mathrm{U}, \mathrm{V}) = (hu, hv)$ is nondivergent.

The momentum equations of the shallow-water model can be recast in transport form:

$$\frac{\partial}{\partial t}(hu) = -\frac{h}{\rho_0}\frac{\partial p}{\partial x} + F_x \tag{7.33a}$$
$$\text{with } F_x = -\frac{\partial}{\partial x}(huu) - \frac{\partial}{\partial y}(hvu) + f\,hv$$
$$\frac{\partial}{\partial t}(hv) = -\frac{h}{\rho_0}\frac{\partial p}{\partial y} + F_y \tag{7.33b}$$
$$\text{with } F_y = -\frac{\partial}{\partial x}(huv) - \frac{\partial}{\partial y}(hvv) - f\,hu.$$

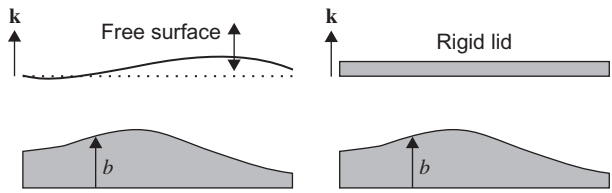


**FIGURE 7.7** A free-surface formulation (left panel) allows the surface to move with the flow, whereas a rigid-lid formulation assumes a fixed surface, under which pressure is not uniform because the "lid" resists any local upward or downward force.

Since we have neglected the variation $\eta$ in surface elevation, we can take in the preceding equations $h = H - b$, a known function of the coordinates $x$ and $y$. The task ahead of us is to find a way to calculate from the preceding two equations (7.33a) and (7.33b), a pressure field $p$ that leads to satisfaction of constraint (7.32). To do so, we have two approaches at our disposal. The first one is based on a diagnostic equation for pressure (Section 7.6), and the second one on a streamfunction formulation (Section 7.7).

## 7.6 NUMERICAL SOLUTION OF THE RIGID-LID PRESSURE EQUATION

The pressure method uses Eqs. (7.33a) and (7.33b) to construct an equation for pressure while enforcing the no-divergence constraint. This is accomplished by adding the $x$-derivative of Eq. (7.33a) to the $y$-derivative of Eq. (7.33b) and exploiting Eq. (7.32) to eliminate the time derivatives. Placing the pressure terms on the left then yields

$$\frac{\partial}{\partial x}\left(\frac{h}{\rho_0}\frac{\partial p}{\partial x}\right) + \frac{\partial}{\partial y}\left(\frac{h}{\rho_0}\frac{\partial p}{\partial y}\right) = \frac{\partial F_x}{\partial x} + \frac{\partial F_y}{\partial y} = Q. \tag{7.34}$$

This equation for pressure is the archetype of a so-called *elliptic equation*.

To complement it, appropriate boundary conditions must be provided. These pressure conditions are deduced from the impermeability of solid lateral boundaries or from the inflow/outflow conditions at open boundaries (see Section 4.6). For example, if the boundary is parallel to the $y$-axis (say $x = x_0$) and is impermeable, we need to impose $hu = 0$ (no normal transport), and the $x$-momentum equation in transport form reduces there to

$$\frac{h}{\rho_0}\frac{\partial p}{\partial x} = F_x, \tag{7.35}$$

while along an impermeable boundary parallel to the $x$-axis (say $y = y_0$), we need to impose $hv = 0$ and obtain from the $y$-momentum equation

$$\frac{h}{\rho_0}\frac{\partial p}{\partial y} = F_y. \tag{7.36}$$

In other words, the normal pressure gradient is given along impermeable boundaries. At inflow/ouflow boundaries, the expression is more complicated but it is still the normal pressure gradient that is imposed. An elliptic equation with the normal derivative prescribed all along the perimeter of the domain is called a Neumann problem.[2]

[2]If the pressure itself had been imposed all along the perimeter of the domain, the problem would have been called a Dirichlet problem.

One and only one condition at every point along all boundaries of the domain is necessary and sufficient to determine the solution of the elliptic equation (7.34). Since the pressure appears only through its derivatives in both the elliptic equation (7.34) and the boundary condition (7.35) and (7.36), the solution is only defined within an additional arbitrary constant, the value of which may be chosen freely without affecting the resulting velocity field. However, there is a natural choice, which is to select the constant so that the pressure has a zero average over the domain. By virtue of $p = \rho_0 g \eta$, this corresponds to stating that $\eta$ has a zero average over the domain.

Numerically, the solution can be sought by discretizing the elliptic equation for pressure across a rectangular box:

$$\begin{aligned} &\frac{1}{\Delta x}\left(h_{i+1/2}\,\frac{\tilde{p}_{i+1,j}-\tilde{p}_{i,j}}{\Delta x}-h_{i-1/2}\,\frac{\tilde{p}_{i,j}-\tilde{p}_{i-1,j}}{\Delta x}\right)\\ &+\frac{1}{\Delta y}\left(h_{j+1/2}\,\frac{\tilde{p}_{i,j+1}-\tilde{p}_{i,j}}{\Delta y}-h_{j-1/2}\,\frac{\tilde{p}_{i,j}-\tilde{p}_{i,j-1}}{\Delta y}\right)=\rho_0 Q_{ij}. \end{aligned} \tag{7.37}$$

This forms a set of linear equations for the $\tilde{p}_{i,j}$ values across the grid, connecting five unknowns at each grid point (Fig. 7.8), a situation already encountered in

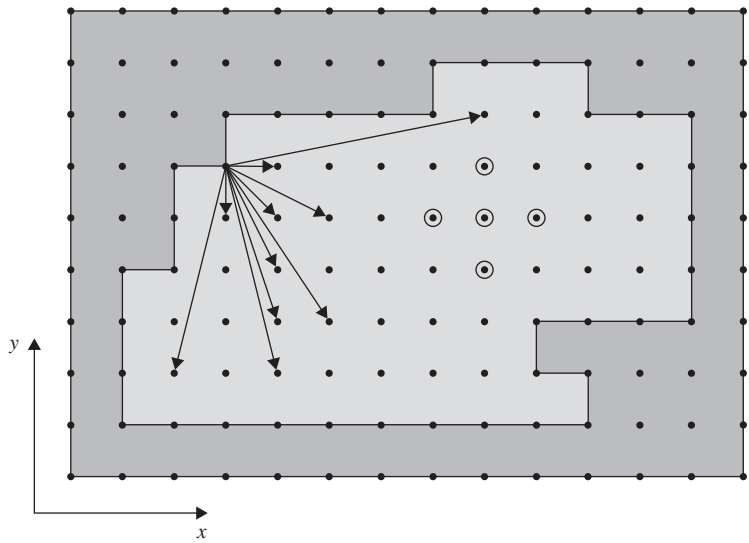


**FIGURE 7.8** Discretization of the two-dimensional elliptic equation. The stencil is a five-point array consisting of the point where the calculation is performed and its four neighbors. These neighboring points are in turn dependent on their respective neighbors, and so on until boundary points are reached. In other words, the value at every point inside the domain is influenced by all other interior and boundary values. Simple accounting indicates that one and only one boundary condition is needed at all boundary points.

the treatment of two-dimensional implicit diffusion (Section 5.6). But there is another circular dependence: The right-hand side $\rho_0 Q_{ij}$ is not known until the velocity components are determined and the determination of these requires the knowledge of the pressure gradient. Because the momentum equations are nonlinear, this is a nonlinear dependence, and the method for constructing and solving a linear system cannot be applied.

The natural way to proceed is to progress incrementally. If we assume that at time level $n$, we have a divergent-free velocity field ($\tilde{u}^n$, $\tilde{v}^n$), we can use Eq. (7.37) to calculate the pressure at the same time level $n$ and use its gradient in the momentum equations to update the velocity components for time level $n+1$. But this offers no guarantee that the updated velocity components will be divergence free, despite the fact that the pressure distribution corresponds to a divergent-free flow field at the previous time level.

Once again, we face a situation in which discretized equations do not inherit certain mathematical properties of the continuous equations. In this case, we used properties of divergence and gradient operators to build a diagnostic pressure equation from the original equations, but these properties are not transferable to the numerical space unless special care is taken.

However, the design of adequate discrete equations can be inspired by the mathematical operations used to reach the pressure equation (7.34): We started with the velocity equation and applied the divergence operator to make appear the divergence of the transport that we then set to zero, and we should perform the same operations in the discrete domain to ensure that at any moment the discrete transport field is nondivergent in a finite volume. This is expressed by discrete volume conservation as

$$\frac{h_{i+1/2}\tilde{u}_{i+1/2} - h_{i-1/2}\tilde{u}_{i-1/2}}{\Delta x} + \frac{h_{j+1/2}\tilde{v}_{j+1/2} - h_{j-1/2}\tilde{v}_{j-1/2}}{\Delta y} = 0. \tag{7.38}$$

Anticipating a *staggered grid* configuration (Fig. 7.9), we realize that it would be natural to calculate for each cell the velocity $\tilde{u}$ at the middle of the left and right interfaces $(i \pm 1/2, j)$ and the other velocity component $\tilde{v}$ at the middle of the top and bottom interfaces $(i, j \pm 1/2)$ so that the divergence may be calculated most naturally in Eq. (7.38). In contrast, $\tilde{p}$ values are calculated at cell centers. Leapfrog time discretization applied to (7.33a) and (7.33b) then

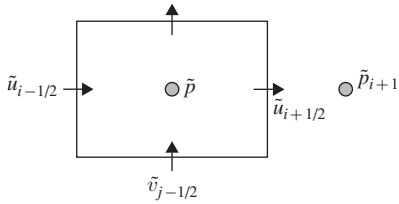


**FIGURE 7.9** Arrangement of numerical unknowns for easy enforcement of numerical volume conservation and pressure-gradient calculations.

provides

$$h_{i+1/2}\tilde{u}^{n+1}_{i+1/2} = h_{i+1/2}\tilde{u}^{n-1}_{i+1/2} + 2\Delta t F_{xi+1/2} - 2\Delta t\, h_{i+1/2}\frac{\tilde{p}_{i+1}-\tilde{p}}{\rho_0 \Delta x} \tag{7.39a}$$

$$h_{j+1/2}\tilde{v}^{n+1}_{j+1/2} = h_{j+1/2}\tilde{v}^{n-1}_{j+1/2} + 2\Delta t F_{yj+1/2} - 2\Delta t\, h_{j+1/2}\frac{\tilde{p}_{j+1}-\tilde{p}}{\rho_0 \Delta y}, \tag{7.39b}$$

in which we omitted for clarity the obvious indices $i$, $j$, and $n$.

Requesting now that the discretized version (7.38) of the nondivergence constraint hold at time level $n+1$, we can eliminate the velocity values at that time level by combining the equations of (7.39) so that these terms cancel out. The result is the sought-after discretized equation for pressure:

$$\begin{aligned}
&\frac{1}{\Delta x}\left(h_{i+1/2}\frac{\tilde{p}_{i+1}-\tilde{p}}{\Delta x} - h_{i-1/2}\frac{\tilde{p}-\tilde{p}_{i-1}}{\Delta x}\right) + \frac{1}{\Delta y}\left(h_{j+1/2}\frac{\tilde{p}_{j+1}-\tilde{p}}{\Delta y} - h_{j-1/2}\frac{\tilde{p}-\tilde{p}_{j-1}}{\Delta y}\right) \\
&\quad = \rho_0\left(\frac{F_{xi+1/2}-F_{xi-1/2}}{\Delta x} + \frac{F_{yj+1/2}-F_{yj-1/2}}{\Delta y}\right) \\
&\qquad + \frac{\rho_0}{2\Delta t}\left(\frac{h_{i+1/2}\tilde{u}^{n-1}_{i+1/2} - h_{i-1/2}\tilde{u}^{n-1}_{i-1/2}}{\Delta x} + \frac{h_{j+1/2}\tilde{v}^{n-1}_{j+1/2} - h_{j-1/2}\tilde{u}^{n-1}_{j-1/2}}{\Delta y}\right),
\end{aligned} \tag{7.40}$$

where once again the obvious indices have been omitted.

It is clear that, up to the last term, this equation is a discrete version of Eq. (7.34) and resembles Eq. (7.37). The difference lies in the last term, which would vanish if the transport field were divergence free at time level $n-1$. We kept that term should the numerical solution of the discrete equation not be exact. Keeping the nonzero discrete divergence at $n-1$ in the equation is a way of applying an automatic correction to the discrete equation in order to insure the nondivergence of the transport at the new time level $n+1$. Neglecting this correction term would result in a gradual accumulation of errors and thus an eventually divergent transport field.

To summarize, the algorithm works as follows: Knowing velocity values at time levels $n$ and $n-1$, we solve Eq. (7.40) iteratively for pressure, which is then used to advance velocity in time using Eqs. (7.39a) and (7.39b). For quickly converging iterations, the pressure calculations can be initialized with the values from the previous time step. This iterative procedure is one of the sources of numerical errors against which the last term of Eq. (7.40) is kept as a precaution.

The discretization shown here is relatively simple, but in the more general case of higher-order methods or other grid configurations, the same approach can be used. We must ensure that the divergence operator applied to the transport field is discretized in the same way as the divergence operator is applied to the pressure gradient. Furthermore, the pressure gradient needs to be discretized in the same way in both the velocity equation and the elliptic pressure equation.

In summary, the derivatives similarly labeled in the equations below must be discretized in identical ways to generate a mathematically coherent scheme:

$$\underbrace{\frac{\partial}{\partial x}}_{(1)}\left(\frac{h}{\rho_0}\underbrace{\frac{\partial p}{\partial x}}_{(3)}\right)+\underbrace{\frac{\partial}{\partial y}}_{(2)}\left(\frac{h}{\rho_0}\underbrace{\frac{\partial p}{\partial y}}_{(4)}\right)=\underbrace{\frac{\partial}{\partial x}}_{(1)}F_x+\underbrace{\frac{\partial}{\partial y}}_{(2)}F_y$$

$$\frac{\partial}{\partial t}(hu) = -\frac{h}{\rho_0}\underbrace{\frac{\partial p}{\partial x}}_{(3)}+F_x$$

$$\frac{\partial}{\partial t}(hv) = -\frac{h}{\rho_0}\underbrace{\frac{\partial p}{\partial y}}_{(4)}+F_y$$

$$\underbrace{\frac{\partial}{\partial x}}_{(1)}(hu)+\underbrace{\frac{\partial}{\partial y}}_{(2)}(hv)=0.$$

It also means one can generally not resort to a "black box" elliptic-equation solver to obtain a pressure field that is used in "hand-made" discrete velocity equations.

## 7.7 NUMERICAL SOLUTION OF THE STREAMFUNCTION EQUATION

Instead of calculating pressure, a second method in use with the rigid-lid approximation is a generalization of the velocity streamfunction $\psi$ to the *volume-transport streamfunction* $\Psi$:

$$hu=-\frac{\partial(h\psi)}{\partial y}=-\frac{\partial\Psi}{\partial y} \tag{7.42a}$$

$$hv=+\frac{\partial(h\psi)}{\partial x}=+\frac{\partial\Psi}{\partial x}. \tag{7.42b}$$

The difference between two isolines of $\Psi$ can be interpreted as the volume transport between those lines, directed with the higher $\Psi$ values to its right.

When transport components are calculated according to Eq. (7.42), volume conservation (7.32) is automatically satisfied, and as shown in Section 6.6, the numerical counterpart can also be divergence free. We may therefore discretize the equation governing $\Psi$ without hesitation, sure that its discrete solution will lead to a well-bahaved discrete velocity field.

To obtain a mathematical equation for the streamfunction, all we have to do is to eliminate the pressure from the momentum equations. This is accomplished by dividing Eqs. (7.33a) and (7.33b) by $h$, differentiating the former by $y$ and the latter by $x$, and finally subtracting one from the other. Replacement of the

transport components $hu$ and $hv$ in terms of the streamfunction then yields

$$\frac{\partial}{\partial t}\left[\frac{\partial}{\partial x}\left(\frac{1}{h}\frac{\partial \Psi}{\partial x}\right)+\frac{\partial}{\partial y}\left(\frac{1}{h}\frac{\partial \Psi}{\partial y}\right)\right]=\frac{\partial}{\partial x}\left(\frac{F_y}{h}\right)-\frac{\partial}{\partial y}\left(\frac{F_x}{h}\right) \qquad (7.43)$$
$$=Q.$$

The right-hand side could be further expanded in terms of the streamfunction, but for the sake of the following discussion it is sufficient to lump all its terms into a single "forcing" term $Q$.

We now consider a leapfrog time discretization or any other time discretization that allows us to write

$$\left[\frac{\partial}{\partial x}\left(\frac{1}{h}\frac{\partial \tilde{\Psi}}{\partial x}\right)^{n+1}+\frac{\partial}{\partial y}\left(\frac{1}{h}\frac{\partial \tilde{\Psi}}{\partial y}\right)^{n+1}\right]=F(\tilde{\Psi}^n,\tilde{\Psi}^{n-1},\ldots). \qquad (7.44)$$

In the case of a leapfrog discretization, the right-hand side is

$$F(\tilde{\Psi}^n,\tilde{\Psi}^{n-1},\ldots)=\left[\frac{\partial}{\partial x}\left(\frac{1}{h}\frac{\partial \tilde{\Psi}}{\partial x}\right)^{n-1}+\frac{\partial}{\partial y}\left(\frac{1}{h}\frac{\partial \tilde{\Psi}}{\partial y}\right)^{n-1}\right] \qquad (7.45)$$
$$+2\Delta t\, Q^n,$$

which can be evaluated numerically knowing $\tilde{\Psi}^n$ and $\tilde{\Psi}^{n-1}$. The problem then amounts to solving Eq. (7.44) for $\tilde{\Psi}^{n+1}$. Again, an elliptic equation must be solved, as for the pressure equation in the previous section, and the same method can be applied.

Differences, other than the terms in the right-hand side, are noteworthy. First, instead of $h$ appearing inside the derivatives, $1/h$ is involved, which increases the role played by the streamfunction derivatives in shallow regions ($h \to 0$, usually near boundaries), possibly amplifying errors on boundary conditions. This is in contrast to the pressure formulation, in which the influence of the vertically integrated pressure gradient decreases in shallow regions. Applications indeed reveal that the solution of the Poisson equation (7.40) is better conditioned and converges better than Eq. (7.44).

A second difference is related to the formulation of boundary conditions. While in the pressure approach imposing zero normal velocity leads to a condition on the normal derivative of pressure, the streamfunction formulation has the apparent advantage of only demanding that the streamfunction be constant along a solid boundary, a Dirichlet condition. A problem arises for ocean models when islands are present within the domain (Fig. 7.10). Knowing that the streamfunction is constant on an impermeable boundary does not tell us what the value of the constant ought to be. This is no small matter because the difference of streamfunction values across a channel defines the volume transport in that

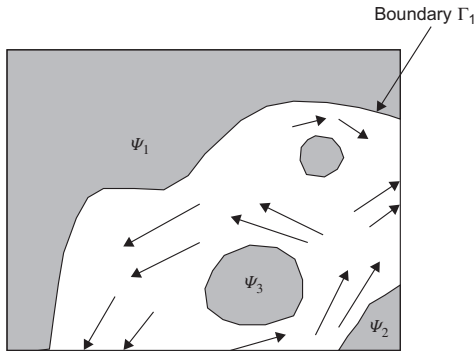


**FIGURE 7.10** Boundary conditions on the streamfunction in an ocean model with islands. The streamfunction value must be prescribed constant along impermeable boundaries. Setting $\Psi_1$ and $\Psi_2$ for the outer boundaries is reasonable and amounts to imposing the total flow across the domain, but setting a priori the value of $\Psi_3$ along the perimeter of an island is in principle not permitted because the flow around the island should depend on the interior solution and its temporal evolution. Clearly, a prognostic equation for the streamfunction value on islands is needed.

channel. Such volume transport should be determined by the dynamics of the flow and not by the modeler's choice.

The streamfunction equation being linear with known right-hand side allows superposition of solutions, and we take one island at a time:

$$\frac{\partial}{\partial x}\left(\frac{1}{h}\frac{\partial \psi_k}{\partial x}\right)+\frac{\partial}{\partial y}\left(\frac{1}{h}\frac{\partial \psi_k}{\partial y}\right)=0 \tag{7.46}$$

with $\psi_k$ set to zero on all boundaries except $\psi_k = 1$ on the boundary for the $k$th island. Each island thus engenders a dimensionless streamfunction $\psi_k(x, y)$ that can be used to construct the overall solution

$$\Psi(x, y, t) = \Psi_f(x, y, t) + \sum_k \Psi_k(t)\psi_k(x, y), \tag{7.47}$$

where $\Psi_f$ is the particular solution of Eq. (7.44) with streamfunction set to zero along all island boundaries and prescribed values along the outer boundaries and wherever the volume flow is known (e.g., at the inflow boundary as depicted in Fig. 7.10). The $\Psi_k(t)$ coefficients are the time-dependent factors by which the island contributions must be multiplied to construct the full solution. What should these factors be is the question.

One possibility is to project the momentum equations onto the direction locally tangent to the island boundary, similarly to what was done to determine the boundary conditions in the pressure formulation. Invoking Stokes theorem on the closed contour formed by the perimeter of the $k$th island then provides an equation including the time derivative $\mathrm{d}\Psi_k/\mathrm{d}t$. Repeating the procedure for each island leads to a linear set of $N$ equations, where $N$ is the number of islands. These equations can then be integrated in time (e.g., Bryan & Cox, 1972). This approach has become less popular over the years for several reasons, among

which is the nonlocal nature of the equations. Indeed, each island equation involves both area and contour integrals all over the domain, causing serious difficulties when the domain is fragmented for calculation on separate computers working in parallel. Synchronization of the information exchange of different integral pieces across computers can be very challenging. Nevertheless, the streamfunction formulation is still available in most large-scale ocean models.

## 7.8 LAPLACIAN INVERSION

Because the inversion of a Poisson-type equation is a recurrent task in numerical models, we now outline some of the methods designed to invert the discrete Poisson equation

$$\frac{\tilde{\psi}_{i+1,j}-2\tilde{\psi}_{i,j}+\tilde{\psi}_{i-1,j}}{\Delta x^2}+\frac{\tilde{\psi}_{i,j+1}-2\tilde{\psi}_{i,j}+\tilde{\psi}_{i,j-1}}{\Delta y^2}=\tilde{q}_{i,j}, \tag{7.48}$$

where the right-hand side is given and $\tilde{\psi}$ is the unknown field.[3] Iterative methods outlined in Section 5.6 using pseudo-time iterations were the first methods used to solve a linear system for $\tilde{\psi}_{i,j}$. The Jacobi method with over-relaxation reads

$$\begin{aligned}\tilde{\psi}_{i,j}^{(k+1)}&=\tilde{\psi}_{i,j}^{(k)}+\omega\epsilon_{i,j}^{(k)}\\ \left(\frac{2}{\Delta x^2}+\frac{2}{\Delta y^2}\right)\epsilon_{i,j}^{(k)}&=\\ \frac{\tilde{\psi}_{i+1,j}^{(k)}-2\tilde{\psi}_{i,j}^{(k)}+\tilde{\psi}_{i-1,j}^{(k)}}{\Delta x^2}&+\frac{\tilde{\psi}_{i,j+1}^{(k)}-2\tilde{\psi}_{i,j}^{(k)}+\tilde{\psi}_{i,j-1}^{(k)}}{\Delta y^2}-\tilde{q}_{i,j},\end{aligned} \tag{7.49}$$

in which the residual $\epsilon$ is used to correct the previous estimate at iteration $(k)$. Taking the relaxation parameter $\omega>1$ (i.e., performing over-relaxation) accelerates convergence toward the solution, at the risk of instability. By considering iterations as evolution in pseudo-time, we can assimilate the parameter $\omega$ to a pseudo-time step and perform a numerical stability analysis. The outcome is that iterations are stable (i.e., they converge) provided $0\leq\omega<2$. In terms of the general iterative solvers of Section 5.6, matrix $\mathbf{B}$ in (5.56) is diagonal. The algorithm requires at least as many iterations to propagate the information once through the domain as they are grid points across the domain. If $M$ is the total number of grid points in the 2D model, then $\sqrt{M}$ is an estimate of the "width" of the grid, and it takes $\sqrt{M}$ iterations to propagate information once from side

[3] Generalization to equations with variable coefficients such as $h$ or $1/h$, as encountered in the preceding two sections for example, is relatively straightforward, and we keep the notation simple here by assuming constant coefficients.

to side. Usually, $M$ iterations are needed for convergence, and the cost rapidly becomes prohibitive with increased resolution.

The finite speed at which information is propagated during numerical iterations does not reflect the actual nature of elliptic equation, the interconnectness of which theoretically implies instantaneous adjustment to any change anywhere, and we sense that we should be able to do better. Because in practice the iterations are only necessary to arrive at the converged solution, we do not need to mimic the process of a time-dependent equation and can tamper with the pseudo-time.

The Gauss-Seidel method with over-relaxation calculates the residual instead as

$$\left(\frac{2}{\Delta x^2}+\frac{2}{\Delta y^2}\right)\epsilon_{i,j}^{(k)} = \frac{\tilde{\psi}_{i+1,j}^{(k)}-2\tilde{\psi}_{i,j}^{(k)}+\tilde{\psi}_{i-1,j}^{(k+1)}}{\Delta x^2}+\frac{\tilde{\psi}_{i,j+1}^{(k)}-2\tilde{\psi}_{i,j}^{(k)}+\tilde{\psi}_{i,j-1}^{(k+1)}}{\Delta y^2}-\tilde{q}_{i,j} \tag{7.50}$$

in which the updated values at the previous neighbors $(i-1, j)$ and $(i, j-1)$ are immediately used (assuming that we loop across the domain with increasing $i$ and $j$). In other words, the algorithm (7.50) does not delay using the most updated values. With this time saving also comes a saving of storage as old values can be replaced by new values as soon as these are calculated. Matrix $\mathbf{B}$ of equation (5.56) is triangular, and the Gauss–Seidel loop (7.50) is the matrix inversion performed by backward substitution. The method is called *SOR*, successive over-relaxation.

The use of the most recent $\tilde{\psi}$ values during the iterations accelerates convergence but not in a drastic way. Only when the relaxation parameter $\omega$ is set at a very particular value can the number of iterations be reduced significantly, from $\mathcal{O}(M)$ down to $\mathcal{O}(\sqrt{M})$ (see Numerical Exercise 7.6). Unfortunately, the optimal value of $\omega$ depends on the geometry and type of boundary conditions, and a small departure from the optimal value quickly deteriorates the convergence rate. As a guideline, the optimal value behaves as

$$\omega \sim 2-\alpha\frac{2\pi}{m} \tag{7.51}$$

for a square and isotropic grid with $m$ grid points in each direction, and with parameter $\alpha = \mathcal{O}(1)$ depending on the nature of the boundary conditions.

Because of its easy implementation, the SOR method was very popular in the early days of numerical modeling, but when vector and, later, parallel computers appeared, some adaptation was required. The recurrence relationships that appear in the loops do not allow to calculate $\tilde{\psi}_{i,j}^{(k+1)}$ before the calculations of $\tilde{\psi}_{i-1,j}^{(k+1)}$ and $\tilde{\psi}_{i,j-1}^{(k+1)}$ are finished, and this prevents independent calculations on parallel processors or vector machines. In response, the so-called *red-black*

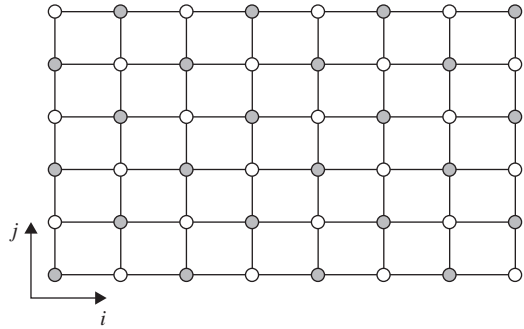


**FIGURE 7.11** To avoid recurrence relationships, the discrete domain is swept by two loops, working on white and gray dots separately. During the loop updating white nodes, only values of the gray nodes are used so that all white nodes can be updated independently and immediately. The reverse holds for the gray nodes in the second loop, and all calculations may be performed in parallel. Because the original algorithm is directly related to the so-called red-black partitioning of trees (e.g., Hageman & Young, 2004), the nodes can be colored accordingly, and "red-black" is the name given to the two-stage sweep mechanism.

methods were developed. These perform two Jacobi iterations on two interlaced grids, nicknamed "red" and "black" (Fig. 7.11).

If we want to reduce further the computational burden associated with the inversion of the Poisson equation, we must exploit the very special nature of (7.48) and the resulting linear system to be solved. For the discrete version (7.48) of the Poisson equation, the matrix $\mathbf{A}$ relating the unknowns, now stored in an array $\mathbf{x}$, is symmetric and positive definite (Numerical Exercise 7.10). In this case, the solution of $\mathbf{Ax}=\mathbf{b}$ is equivalent to solving the minimization of

$$J=\frac{1}{2}\mathbf{x}^{\mathsf{T}}\mathbf{Ax}-\mathbf{x}^{\mathsf{T}}\mathbf{b} \tag{7.52}$$

$$\nabla_x J=\mathbf{Ax}-\mathbf{b} \tag{7.53}$$

with respect to $\mathbf{x}$. We then have to search for minima rather than to solve a linear equation and, though apparently more complicated, the task can also be tackled by iterative methods. The minimum of $J$ is reached when the gradient with respect to $\mathbf{x}$ is zero: $\nabla_x J=0$. This is the case when the residual $\mathbf{r}=\mathbf{Ax}-\mathbf{b}$ is zero, that is, when the linear problem is solved.

The use of a minimization approach (e.g., Golub & Van Loan, 1990) instead of a linear-system solver relies on the possibility of using efficient minimization methods. The gradient of $J$, the residual, is easily calculated and only takes $4M$ operations for the matrix $\mathbf{A}$ arising from the discrete Poisson equation. The value of $J$, if desired, is also readily obtained by calculating two scalar products involving the already available gradient. A standard minimization method used in optimization problems is to minimize the residual $J$ by following its gradient. In this method, called the *steepest descent* method, a better estimate

of $\mathbf{x}$ is sought in the direction in which $J$ decreases fastest. Starting from $\mathbf{x}_0$ and associated residual $\mathbf{r} = \mathbf{A}\mathbf{x}_0 - \mathbf{b}$, a better estimate of $\mathbf{x}$ is sought as

$$\mathbf{x} = \mathbf{x}_0 - \alpha \mathbf{r}, \tag{7.54}$$

which is reminiscent of a relaxation method. The parameter $\alpha$ is then chosen to minimize $J$. Because the form is quadratic in $\alpha$, this can be achieved easily (see Numerical Exercise 7.7) by taking

$$\alpha = \frac{\mathbf{r}^{\mathsf{T}}\mathbf{r}}{\mathbf{r}^{\mathsf{T}}\mathbf{A}\mathbf{r}} \tag{7.55}$$

which, because $\mathbf{A}$ is positive definite, can always be calculated as long as the residual is nonzero. If the residual vanishes, iterations can be stopped because the solution has been found. Otherwise, from the new estimate $\mathbf{x}$, a new residual and gradient are computed, and iterations proceed:

Initialize by first guess $\mathbf{x}^{(0)} = \mathbf{x}_0$

Loop on increasing $k$ until the residual $\mathbf{r}$ is small enough

$$\mathbf{r} = \mathbf{A}\mathbf{x}^{(k)} - \mathbf{b}$$

$$\alpha = \frac{\mathbf{r}^{\mathsf{T}}\mathbf{r}}{\mathbf{r}^{\mathsf{T}}\mathbf{A}\mathbf{r}}$$

$$\mathbf{x}^{(k+1)} = \mathbf{x}^{(k)} - \alpha \mathbf{r}$$

End of loop on $k$.

where residual and optimal descent parameter $\alpha$ change at each iteration. It is interesting to note that the residuals of two successive iterations are orthogonal to each other (Numerical Exercise 7.7).

Although very natural, the approach does not converge rapidly, and *conjugate gradient* methods have been developed to provide better convergence rates. In these methods, the direction of progress is no longer the direction of the steepest descent but is prescribed from among a set, noted $\mathbf{e}_i$. We then look for the minimum along these possible directions:

$$\mathbf{x} = \mathbf{x}_0 - \alpha_1 \mathbf{e}_1 - \alpha_2 \mathbf{e}_2 - \alpha_3 \mathbf{e}_3 - \cdots - \alpha_M \mathbf{e}_M. \tag{7.56}$$

If there are $M$ vectors $\mathbf{e}_i$, chosen to be linearly independent, minimization with respect to the $M$ parameters $\alpha_i$ will yield the exact minimum of $J$. So, instead of searching for the $M$ components of $\mathbf{x}$, we search for the $M$ parameters $\alpha_i$ leading to the optimal state $\mathbf{x}$. This solves the linear system exactly. A simplification in the calculations arises if we choose

$$\mathbf{e}_i^{\mathsf{T}}\mathbf{A}\mathbf{e}_j = 0 \quad \text{when} \quad i \neq j \tag{7.57}$$

because in this case the quadratic form $J$ takes the form

$$\begin{aligned} J = & \frac{1}{2}\mathbf{x}_0^{\mathsf{T}}\mathbf{A}\mathbf{x}_0 - \mathbf{x}_0^{\mathsf{T}}\mathbf{b} \\ & + \frac{\alpha_1^2}{2}\mathbf{e}_1^{\mathsf{T}}\mathbf{A}\mathbf{e}_1 - \alpha_1\mathbf{e}_1^{\mathsf{T}}\left(\mathbf{A}\mathbf{x}_0 - \mathbf{b}\right) \\ & + \frac{\alpha_2^2}{2}\mathbf{e}_2^{\mathsf{T}}\mathbf{A}\mathbf{e}_2 - \alpha_2\mathbf{e}_2^{\mathsf{T}}\left(\mathbf{A}\mathbf{x}_0 - \mathbf{b}\right) \\ & + \cdots \\ & + \frac{\alpha_M^2}{2}\mathbf{e}_M^{\mathsf{T}}\mathbf{A}\mathbf{e}_M - \alpha_M\mathbf{e}_M^{\mathsf{T}}\left(\mathbf{A}\mathbf{x}_0 - \mathbf{b}\right). \end{aligned} \tag{7.58}$$

This expression is readily minimized with respect to each parameter $\alpha_k$ and yields, with $\mathbf{r}_0 = \mathbf{A}\mathbf{x}_0 - \mathbf{b}$,

$$\alpha_k = \frac{\mathbf{e}_k^{\mathsf{T}}\mathbf{r}_0}{\mathbf{e}_k^{\mathsf{T}}\mathbf{A}\mathbf{e}_k}, \quad k = 1, \ldots, M \tag{7.59}$$

In other words, to reach the global minimum and thus the solution of the linear system, we simply have to minimize each term individually. However, the difficulty is that the construction of the set of directions $\mathbf{e}_k$ is complicated. Hence, the idea is to proceed step by step and construct the directions as we iterate, with the plan of stopping iterations when residuals have become small enough. We can start with a first arbitrary direction, typically the steepest descent $\mathbf{e}_1 = \mathbf{A}\mathbf{x}_0 - \mathbf{b}$. Then, once we have a set of $k$ directions that satisfy Eq. (7.57), we only minimize along direction $\mathbf{e}_k$ by Eq. (7.59):

$$\mathbf{x}^{(k)} = \mathbf{x}^{(k-1)} - \alpha_k\mathbf{e}_k. \tag{7.60}$$

This leads to a new residual $\mathbf{r}_k = \mathbf{A}\mathbf{x}^{(k)} - \mathbf{b}$

$$\begin{aligned} \mathbf{r}_k &= \mathbf{r}_{k-1} - \alpha_k\mathbf{A}\mathbf{e}_k \\ &= \mathbf{r}_0 - \alpha_1\mathbf{A}\mathbf{e}_1 - \alpha_2\mathbf{A}\mathbf{e}_2 - \cdots - \alpha_k\mathbf{A}\mathbf{e}_k. \end{aligned} \tag{7.61}$$

This shows that, instead of calculating $\alpha_k$ according to Eq. (7.59), we can use

$$\alpha_k = \frac{\mathbf{e}_k^{\mathsf{T}}\mathbf{r}_{k-1}}{\mathbf{e}_k^{\mathsf{T}}\mathbf{A}\mathbf{e}_k} \tag{7.62}$$

because of property (7.57). We can interpret this result together with (7.61) by showing that the successive residuals are orthogonal to all previous search directions $\mathbf{e}_i$ so that no new search in those directions is needed. Expression (7.62) is also more practical because it requires the storage of only the residual calculated at the previous iteration. The construction of the next direction $\mathbf{e}_{k+1}$ is then performed by a variation of the Gram–Schmidt orthogonalization process of a

series of linearly independent vectors. The conjugate gradient method chooses for this set of vectors the residuals already calculated, which can be shown to be orthogonal to one another and hence linearly independent. When applying the Gram–Schmidt orthogonalization in the sense of Eq. (7.57), it turns out that the new direction $\mathbf{e}_{k+1}$ is surprisingly easy to calculate in terms of the last residuals and search direction (e.g., Golub & Van Loan, 1990):

$$\mathbf{e}_{k+1} = \mathbf{r}_k + \frac{\|\mathbf{r}_k\|^2}{\|\mathbf{r}_{k-1}\|^2}\mathbf{e}_k \tag{7.63}$$

from which we can proceed to the next step. The algorithm is therefore only slightly more complicated than the steepest-descent method, and we note that we no longer need to store all residuals or search directions, not even intermediate values of $\mathbf{x}$. Only the most recent one needs to be stored at any moment for the following algorithm:

```
Initialize by first guess
```
$$\mathbf{x}^{(0)} = \mathbf{x}_0, \quad \mathbf{r}_0 = \mathbf{A}\mathbf{x}_0 - \mathbf{b}, \quad \mathbf{e}_1 = \mathbf{r}_0, \quad s_0 = \|\mathbf{r}_0\|^2$$
```
Loop on increasing k until the residual r is small enough
```
$$\alpha_k = \frac{\mathbf{e}_k^{\mathrm{T}}\mathbf{r}_{k-1}}{\mathbf{e}_k^{\mathrm{T}}\mathbf{A}\mathbf{e}_k}$$
$$\mathbf{x}^{(k)} = \mathbf{x}^{(k-1)} - \alpha_k\mathbf{e}_k$$
$$\mathbf{r}_k = \mathbf{r}_{k-1} - \alpha_k\mathbf{A}\mathbf{e}_k$$
$$s_k = \|\mathbf{r}_k\|^2$$
$$\mathbf{e}_{k+1} = \mathbf{r}_k + \frac{s_k}{s_{k-1}}\mathbf{e}_k$$
```
End of loop on k.
```

Because we minimize independent terms, we are sure to reach the minimum of $J$ in $M$ steps, within rounding errors. For the conjugate-gradient method, the exact solution is therefore obtained within $M$ iterations, and the overall cost of our special sparse matrix inversion arising from the two-dimensional discrete Poisson equation behaves as $M^2$. However, there is no need to find the exact minimum, and in practice, only a certain number of successive minimizations are necessary, and convergence is generally obtained within $M^{3/2}$ operations. This does not seem an improvement over the optimal over-relaxation, but the conjugate-gradient method is generally robust and has no need of an over-relaxation parameter. If in addition a proper preconditioning is applied, it can lead to spectacular convergence rates.

Preconditioning needs to preserve the symmetry of the problem and is performed by introducing a sparse triangular matrix $\mathbf{L}$ and writing the original problem as

$$\mathbf{L}^{-1}\mathbf{A}\mathbf{L}^{-\mathrm{T}}\mathbf{L}^{\mathrm{T}}\mathbf{x} = \mathbf{L}^{-1}\mathbf{b}, \tag{7.64}$$

so that we now work with the new unknown $\mathbf{L}^{\mathrm{T}}\mathbf{x}$ and modified matrix $\mathbf{L}^{-1}\mathbf{A}\mathbf{L}^{-\mathrm{T}}$. This matrix is symmetric, and, if $\mathbf{L}$ is chosen correctly, also positive definite if $\mathbf{A}$ is. The resulting algorithm, involving the modified matrix and unknown, is very close to the original conjugate-gradient algorithm after clever rearrangement of the matrix-vector products. The only difference is the appearance of $\mathbf{M}^{-1}\mathbf{r}$, where $\mathbf{M}^{-1} = \mathbf{L}^{-\mathrm{T}}\mathbf{L}^{\mathrm{T}}$. Because $\mathbf{u} = \mathbf{M}^{-1}\mathbf{r}$ is the solution of $\mathbf{M}\mathbf{u} = \mathbf{r}$, the sparseness and triangular nature of $\mathbf{L}$ allows us to perform this operation quite efficiently. If $\mathbf{L} = \mathbf{C}$ is obtained from a Cholesky decomposition of the symmetric positive-definite matrix $\mathbf{A} = \mathbf{C}\mathbf{C}^{\mathrm{T}}$, where $\mathbf{C}$ is a triangular matrix, a single step of the conjugate-gradient method would suffice because the inversion of $\mathbf{A}$ would be directly available. For this reason, $\mathbf{L}$ is often constructed by the Cholesky decomposition but with incomplete and cost-effective calculations, imposing on $\mathbf{L}$ a given sparse pattern. This leads to the incomplete Cholesky preconditioning[4] and reduces the cost of the decomposition but increases the number of iterations needed compared to a situation in which the full Cholesky decomposition is available. On the other hand, it generally reduces the number of iterations compared to the version without preconditioning. An optimum is therefore to be found in the amount of preconditioning, and the particular choice of preconditioning is problem dependent. Stability of the iterations might be an occasional problem.

Most linear-algebra packages contain conjugate-gradient methods including generalizations to solve nonsymmetric problems. In this case, we can consider the augmented (double) problem

$$\begin{pmatrix} 0 & \mathbf{A} \\ \mathbf{A}^{\mathrm{T}} & 0 \end{pmatrix} \begin{pmatrix} \mathbf{y} \\ \mathbf{x} \end{pmatrix} = \begin{pmatrix} \mathbf{b} \\ \mathbf{c} \end{pmatrix} \tag{7.65}$$

which is symmetric and possesses the same solution $\mathbf{x}$.

More efficient solution methods for special linear systems, such as our Poisson equation, exist and exhibit a close relationship with Fast Fourier Transforms (FFT, see Appendix C). The cyclic block reduction methods (e.g., Ferziger & Perić, 1999), for example, can be applied when the discretization constants are uniform and boundary conditions simple. But in such a case, we could also use a spectral method coupled with FFT for immediate inversion of the Laplacian operator (see Section 18.4). In these methods, costs can be reduced down to $M \log M$.

Finally, the most efficient methods for very large problems are *multigrid* methods. These start from the observation that the pseudo-evolution approach mimics diffusion, which generally acts more efficiently at smaller scales [see damping rates of discrete diffusion operators (5.34)], leaving larger scales to converge more slowly. But these larger scales can be made to appear as

[4]More generally, an incomplete **LU** decomposition approximates any matrix $\mathbf{A}$ by the product of lower and upper sparse triangular matrices.

relatively shorter scales on a grid with wider grid spacing so that their convergence can be accelerated (using, incidentally, a larger pseudo-time step). Thus, introducing a hierarchy of grids, as a *multigrid* method does, accelerates convergence by iterating on different grids for different length scales. Typically, the method begins with a very coarse grid, on which a few iterations lead to a good estimate of the broad shape of the solution. This solution is then interpolated onto a finer grid on which several more iterations are performed, and so on down to the ultimate resolution of interest. The iterations may also be redone on the coarser grids after some averaging to estimate the broad solution from the finer grid. Multigrid methods, therefore, cycle through different grids (e.g., Hackbusch, 1985), and the art is to perform the right number of iterations on each grid and to choose wisely the next grid on which to iterate (finer or coarser). For well-chosen strategies, the number of operations required for convergence behaves asymptotically as $M$, and multigrid methods are therefore the most effective ones for very large problems. Iterations on each of the grids may be of red-black type with over-relaxation or any other method with appropriate convergence properties.

We only scratched here the surface of the problem of solving large and sparse linear algebraic systems to give a flavor of the possible approaches, and the reader should be aware that there is a large number of numerical solvers available for specific problems. Since these are optimized for specific computer hardware, the practical and operational task of large-system inversion of the discrete Poisson equation should be left to libraries provided with the computing system available. Only the choice of when to stop the iterations and the proper preconditioning strategy should be left to the modeler.

## ANALYTICAL PROBLEMS

**7.1.** A laboratory experiment is conducted in a cylindrical tank 20 cm in diameter, filled with homogeneous water (15 cm deep at the center) and rotating at 30 rpm. A steady flow field with maximum velocity of 1 cm/s is generated by a source-sink device. The water viscosity is $10^{-6}\,\mathrm{m}^2/\mathrm{s}$. Verify that this flow field meets the conditions of geostrophy.

**7.2.** (Generalization of the Taylor–Proudman theorem) By reinstating the $f_*$–terms of equations (3.19) and (3.22) into (7.2a) and (7.2c) show that motions in fluids rotating rapidly around an axis not parallel to gravity exhibit columnar behavior in the direction of the axis of rotation.

**7.3.** Demonstrate the assertion made at the end of Section 7.2, namely, that geostrophic flows between irregular bottom and top boundaries are constrained to be directed along lines of constant fluid depth.

**7.4.** Establish Eq. (7.22) for the evolution of a parcel's horizontal cross section from first principles.

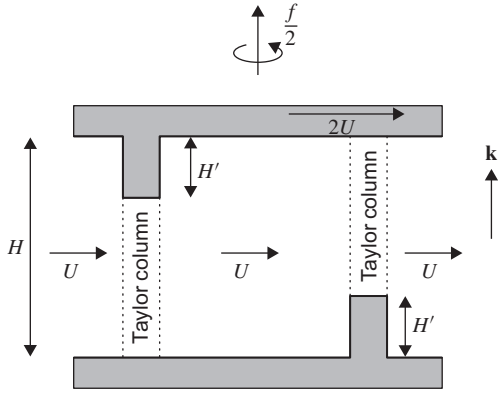


**FIGURE 7.12** Schematic view of a hypothetical system as described in Analytical Problem 7.5.

**7.5.** In a fluid of depth $H$ rapidly rotating at the rate $f/2$ (Fig. 7.12), there exists a uniform flow $U$. Along the bottom (fixed), there is an obstacle of height $H'$ ($<H/2$), around which the flow is locally deflected, leaving a quiescent Taylor column. A rigid lid, translating in the direction of the flow at speed $2U$, has a protrusion identical to the bottom obstacle, also locally deflecting the otherwise uniform flow and entraining another quiescent Taylor column. The two obstacles are aligned with the direction of motion so that there will be a time when both are superimposed. Assuming that the fluid is homogeneous and frictionless, what do you think will happen to the Taylor columns?

**7.6.** As depicted in Fig. 7.13, a vertically uniform but laterally sheared coastal current must climb a bottom escarpment. Assuming that the jet velocity still vanishes offshore, determine the velocity profile and the width of the jet downstream of the escarpment using $H_1 = 200\,\text{m}$, $H_2 = 160\,\text{m}$, $U_1 = 0.5\,\text{m/s}$, $L_1 = 10\,\text{km}$, and $f = 10^{-4}\,\text{s}^{-1}$. What would happen if the downstream depth were only 100 m?

**7.7.** What are the differences in dynamic pressure across the coastal jet of Problem 7.6 upstream and downstream of the escarpment? Take $H_2 = 160\,\text{m}$ and $\rho_0 = 1022\,\text{kg/m}^3$.

**7.8.** In Utopia, a narrow 200-m-deep channel empties in a broad bay of varying bottom topography (Fig. 7.14). Trace the path to the sea and the velocity profile of the channel outflow. Take $f = 10^{-4}\,\text{s}^{-1}$. Solve only for straight stretches of the flow and ignore corners.

**7.9.** A steady ocean current of uniform potential vorticity $q = 5 \times 10^{-7}\,\text{m}^{-1}\text{s}^{-1}$ and volume flux $Q = 4 \times 10^5\,\text{m}^3/\text{s}$ flows along isobaths of a uniformly sloping bottom (with bottom slope $S = 1$ m/km). Show that the velocity profile across the current is parabolic. What are the width

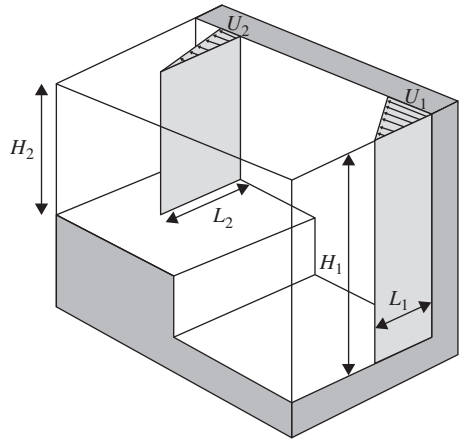


**FIGURE 7.13** A sheared coastal jet negotiating a bottom escarpment (Problem 7.6).

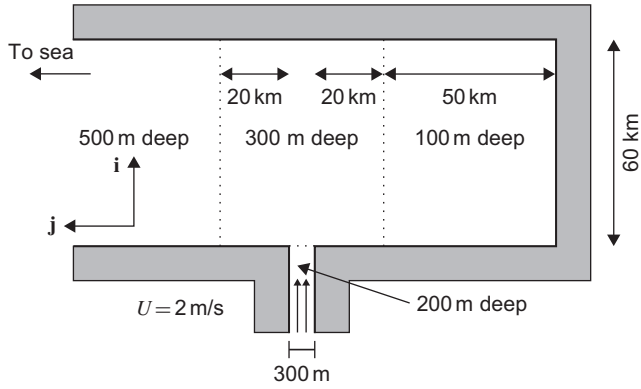


**FIGURE 7.14** Geometry of the idealized bay and channel mentioned in Analytical Problem 7.8.

of the current and the depth of the location of maximum velocity? Take $f = 7 \times 10^{-5}\ \mathrm{s}^{-1}$.

**7.10.** Show that the rigid-lid approximation can also be obtained by assuming that the vertical velocity at top is much smaller than at the bottom. Establish the necessary scaling conditions that support your assumptions.

## NUMERICAL EXERCISES

**7.1.** An atmospheric pressure field $p$ over a flat bottom is given on a rectangular grid according to

$$p_{i,j} = P_H \exp(-r^2/L^2) + p_\epsilon\, \xi_{i,j} \quad r^2 = (x_i - x_c)^2 + (y_j - y_c)^2 \qquad (7.66)$$

where $\xi$ is a normal (Gaussian) random variable of zero mean and unit standard deviation. The high pressure anomaly is of $P_H = 40$ hPa and its radius $L = 1000$ km. For the noise level, take $p_\epsilon = 5$ hPa. Use a rectangular grid centered around $x_c$, $y_c$ with a uniform grid spacing $\Delta x = \Delta y = 50$ km. Calculate and plot the associated geostrophic currents for $f = 10^{-4}\,\mathrm{s}^{-1}$. To which extent is volume conservation satisfied in your finite-difference scheme? What happens if $p_\epsilon = 10$ hPa or $\Delta x = \Delta y = 25$ km? Can you interpret your finding?

**7.2.** Open file `madt_oer_merged_h_18861.nc` and use the sea surface height reconstructed from satellite data to calculate geostrophic ocean currents around the Gulf Stream. Data can be read with `topexcirculation.m`. For conversion from latitude and longitude to local Cartesian coordinates, 1° latitude = 111 km and 1° longitude = 111 km × cos (latitude). (*Altimeter data are products of the CLS Space Oceanography Division; see also Ducet, Le Traon & Reverdin, 2000*).

**7.3.** Use the meteorological pressure field at sea level to calculate geostrophic winds over Europe. First use the December 2000 monthly average sea-level pressure, then look at daily variations. `Era40.m` will help you read the data. Take care of using the local Coriolis parameter value. Geographical distances can be calculated from the conversion factors given in Numerical Exercise 7.2.

What happens if you redo your calculations in order to plan your sailing trip in the northern part of Lake Victoria? (*ECMWF ERA-40 data were obtained from the ECMWF data server*)

**7.4.** Use the red-black approach to calculate the numerical solution of Eq. (7.48) inside the basin depicted in Fig. 7.15, with $\tilde{q}_{i,j} = -1$ on the right-hand side of the equation and $\tilde{\psi}_{i,j} = 0$ along all boundaries. Implement a stopping criterion based on a relative measure of the residual compared to $\mathbf{b}$.

**7.5.** Use the conjugate-gradient implementation called in `testpcg.m` to solve the problem of Numerical Exercise 7.4 with improved convergence.

**7.6.** Redo Numerical Exercise 7.4 with the Gauss–Seidel approach using over-relaxation and several values of $\omega$ between 0.7 and 1.999. For each value of $\omega$, start from zero and converge until reaching a preset threshold for the residual. Plot the required number of iterations until convergence as a function of $\omega$. Design a numerical tool to find the optimal value of $\omega$ numerically. Then repeat the problem by varying the spatial resolution, taking successively 20, 40, 60, 80, and 100 grid points in each direction. Look at the number of iterations and the optimal value of $\omega$ as functions of resolution.

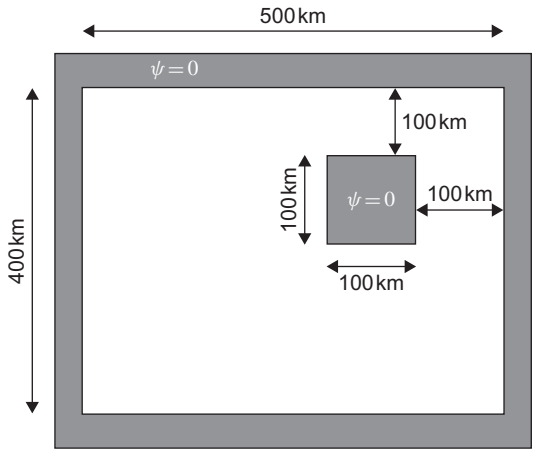


**FIGURE 7.15** Geometry of the idealized basin mentioned in Numerical Exercise 7.4.

**7.7.** Prove that the parameter $\alpha$ given by Eq. (7.55) leads to a minimum of $J$ defined in Eq. (7.52), for a given starting point and fixed gradient $\mathbf{r}$. Also prove that at the next iteration of the steepest-descent method, the new residual is orthogonal to the previous residual. Implement the steepest-descent algorithm to find the minimum of Eq. (7.52) with

$$\mathbf{A} = \begin{pmatrix} 3 & 1 \\ 1 & 1 \end{pmatrix}, \quad \mathbf{b} = \begin{pmatrix} 6 \\ 2 \end{pmatrix} \tag{7.67}$$

starting at the origin of the axes. Observe the successive approximations obtained by the method. (*Hint*: In the plane defined by the two unknowns, plot isolines of $J$ and plot the line connecting the successive approximations to the solution. Make several zooms near the solution point.)

**7.8.** Write a general solver for the Poisson equation as a Matlab$^{TM}$ function. Provide for masked grids and a variable rectangular grid such that $\Delta x$ depends on $i$ and $\Delta y$ on $j$. Also permit variable coefficients in the Laplacian operator, as found in Eq. (7.44) and apply to the following situation.

In shallow, wind-driven basins, such as small lakes and lagoons, the flow often strikes a balance between the forces of surface wind, pressure gradient, and bottom friction. On defining a streamfunction $\psi$ and eliminating the pressure gradient, one obtains for steady flow (Mathieu, Deleersnijder, Cushman-Roisin, Beckers & Bolding, 2002):

$$\frac{\partial}{\partial x}\left(\frac{2\nu_E}{h^3}\frac{\partial \psi}{\partial x}\right) + \frac{\partial}{\partial y}\left(\frac{2\nu_E}{h^3}\frac{\partial \psi}{\partial y}\right) = \frac{\partial}{\partial y}\left(\frac{\tau^x}{\rho_0 h}\right) - \frac{\partial}{\partial x}\left(\frac{\tau^y}{\rho_0 h}\right), \tag{7.68}$$

where $\nu_E$ is the vertical eddy viscosity, $h(x, y)$ is the local bottom depth, and $(\tau^x, \tau^y)$ the components of the surface wind stress. In the application,

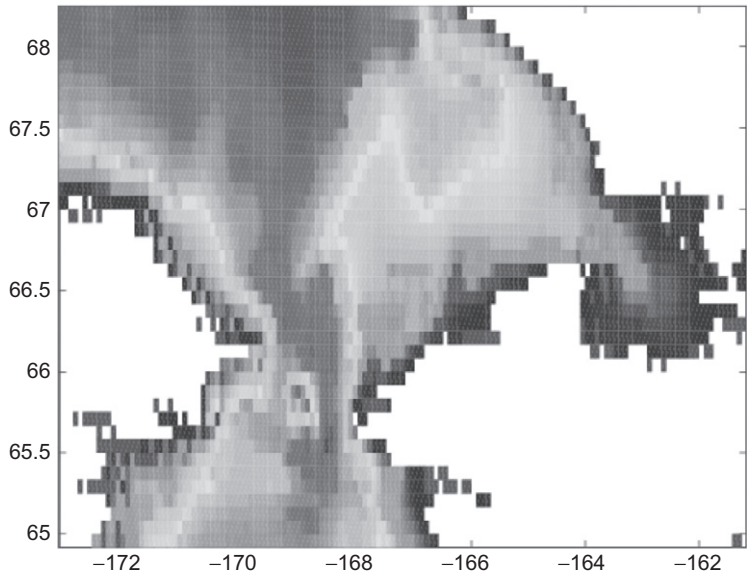


**FIGURE 7.16** Model of the Bering Sea for Numerical Exercise 7.9. For the calculation of the streamfunction, assume that West of $-169°$ longitude all land points have a prescribed streamfunction $\Psi_1 = 0$ and those to the East $\Psi_2 = 0.8$ Sv (1 Sv $= 10^6$ m$^3$/s). For convenience, you may consider closing the western and eastern boundary completely and imposing a zero normal derivative of $\Psi$ along the open boundaries.

take $\nu_E = 10^{-2}$ m$^2$/s, $\rho_0 = 1000$ kg/m$^3$, $h(x, y) = 50 - (x^2 + 4y^2/10)$ (in m, with $x$ and $y$ in km), $\tau^x = 0.1$ N/m$^2$, and $\tau^y = 0$ within the elliptical domain $x^2 + 4y^2 \leq 400$ km$^2$.

**7.9.** Use the tool developed in Numerical Exercise 7.8 to simulate the stationary flow across the Bering Sea, assuming the right-hand side of Eq. (7.68) is zero. Use `beringtopo.m` to read the topography of Fig. 7.16. To pass from latitude and longitude to Cartesian coordinates, use the conversion factors given in Numerical Exercise 7.2 but with cos(latitude) taken as cos(66.5°N) to obtain a rectangular grid. Compare your solution to the case of uniform average depth in place of the real topography, maintaining the same land mask.

**7.10.** Prove that matrix $\mathbf{A}$ arising from the discretization of Eq. (7.48) is symmetric and positive definite if we change the sign of each side. Show also that the latter property ensures $\mathbf{z}^T\mathbf{A}\mathbf{z} > 0$ for any $\mathbf{z} \neq 0$.

**7.11.** Calculate the amplification factor of Gauss–Seidel iterations including over-relaxation. Can you infer the optimal over-relaxation coefficient for Dirichlet conditions? (*Hint*: The optimal parameter will ensure that the slowest damping is accomplished as fast as possible.)

## Geoffrey Ingram Taylor
## 1886–1975

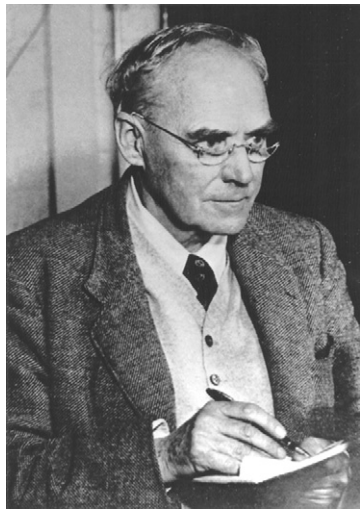

Considered one of the great physicists of the twentieth century, Sir Geoffrey Taylor contributed enormously to our understanding of fluid dynamics. Although he did not envision the birth and development of geophysical fluid dynamics, his research on rotating fluids laid the foundation for the discipline. His numerous contributions to science also include seminal work on turbulence, aeronautics, and solid mechanics. With a staff consisting of a single assistant engineer, he maintained a very modest laboratory, constantly preferring to undertake entirely new problems and to work alone. (*Photo courtesy of Cambridge University Press*)

## James Cyrus McWilliams
## 1946–

A student of George Carrier at Harvard University, James McWilliams is a pioneer in the synthesis of mathematical theory and computational simulation in geophysical fluid dynamics. A central theme of his research is how advection produces the peculiar combinations of global order and local chaos—and vice versa—evident in oceanic currents, as well as analogous phenomena in atmospheric and astrophysical flows. His contributions span a formidable variety of topics across the disciplines of rotating and stratified flows, waves, turbulence, boundary layers, oceanic general circulation, and computational methods.

McWilliams' scientific style is the pursuit of phenomenological discovery in the virtual reality of simulations, leading, "on good days," to dynamical understanding and explanation and to confirmation in nature. (*Photo credit: J. C. McWilliams*)